RESEARCH ARTICLE SUMMARY

SYNTHETIC BIOLOGY

# Monitoring of cell-cell communication and contact history in mammals

**Shaohua Zhang†, Huan Zhao†, Zixin Liu, Kuo Liu, Huan Zhu, Wenjuan Pu, Lingjuan He, Rong A. Wang, Bin Zhou***

**INTRODUCTION:** Cell-cell communication through direct contact is pervasive in multicellular organisms and is essential in many fundamental biological processes. The ability to experimentally track such cell-cell communication signaling could substantially advance our understanding of diverse biological processes from embryogenesis to tumorigenesis. The existing technologies are not suitable to monitor and trace cell-cell contact for long-term in vivo studies, because many biological processes such as embryogenesis, tumorigenesis, and tissue regeneration develop over time after the initial cell-cell contact.

**RATIONALE:** The Notch pathway transmits signaling through direct cell-cell contact in many cellular processes during development and homeostasis. In the canonical Notch pathway, upon cell contact, the Notch ligand on one cell binds to the Notch receptor on another cell to trigger a signaling pathway that leads to transcription activation of particular genes. To understand the dynamic in vivo cell-cell communications over time, we developed an intercellular genetic approach using the synthetic Notch pathway (synNotch) that converts a cellular contact event into a controllable transcriptional program. We engineered in mice an artificial Notch ligand, a membrane-tethered green fluorescent protein (GFP), into one cell type (the sender cell) and an artificial receptor in which the extracellular and intracellular domains of Notch were replaced with an anti-GFP nanobody and the tetracycline transactivator, respectively, into another cell type (the receiver cell). Contact between the sender and receiver cells triggered synNotch signaling that activated the downstream transcriptional programs in the receiver cell in vivo. To reveal the ongoing cell-cell contact, as reflected by synNotch activation in a receiver cell after direct contact with a sender cell, we used a tet-off system to express detectable reporters. To trace cell contact history, we used the Cre-loxP system to genetically fate map receiver cells, along with their progenies, permanently after cell contact.

**RESULTS:** In the intercellular genetic system, we demonstrated that endothelial cells (receiver cells) in the developing heart were genetically labeled after contact with neighboring cardiomyocytes (sender cells). The endothelial cells that had contact with cardiomyocytes in early embryogenesis were permanently tagged with the genetic reporter. Their progenies migrated into liver and subsequently formed a substantial portion of the vasculature there, suggesting that part of the liver vasculature originates from the developing heart during embryogenesis. Application of these synNotch mice in tumorigenesis revealed the contact history between tumor cells (sender cells) and endothelial cells (receiver cells) during tumor growth and revealed that tumor vessels not only expanded within the tumor but also outgrew into the periphery of the tumor and had strong angiogenic properties. Upon contacting tumor cells, these endothelial cells gained properties in angiogenic, migratory, and inflammatory responses. Additionally, we generated mice for Cre-induced synNotch ligand or receptor expression, enabling broadly applicable approaches for genetic labeling of cell-cell contact and study of cell contact signaling in vivo. Engineering both the synNotch ligand and receptor, as well as different genetic readouts, in one mouse, we demonstrated simultaneous yet distinct recording of not only ongoing cell-cell contact but also historical cell-cell contact.

**CONCLUSION:** Our work provides a genetic system for recording cell-cell contact and cell contact history in vivo. The implications of our findings are that endothelial cells in the developing heart migrate and contribute to the liver vasculature, whereas endothelial cells in tumors not only expand within the tumor but also grow outward into the boundary-adjacent normal tissue with robust angiogenesis. The suite of new synNotch mouse lines provides a toolbox for genetic labeling and tracing of contacts between any cell type, offering a useful approach for studying dynamic in vivo cell-cell communications and the resulting cell fate plasticity in diverse life science fields. ■

The list of author affiliations is available in the full article online.
*Corresponding author. Email: zhoubin@sibs.ac.cn
†These authors contributed equally to this work.
Cite this article as S. Zhang *et al.*, *Science* **378**, eabo5503 (2022). DOI: 10.1126/science.abo5503

READ THE FULL ARTICLE AT
https://doi.org/10.1126/science.abo5503

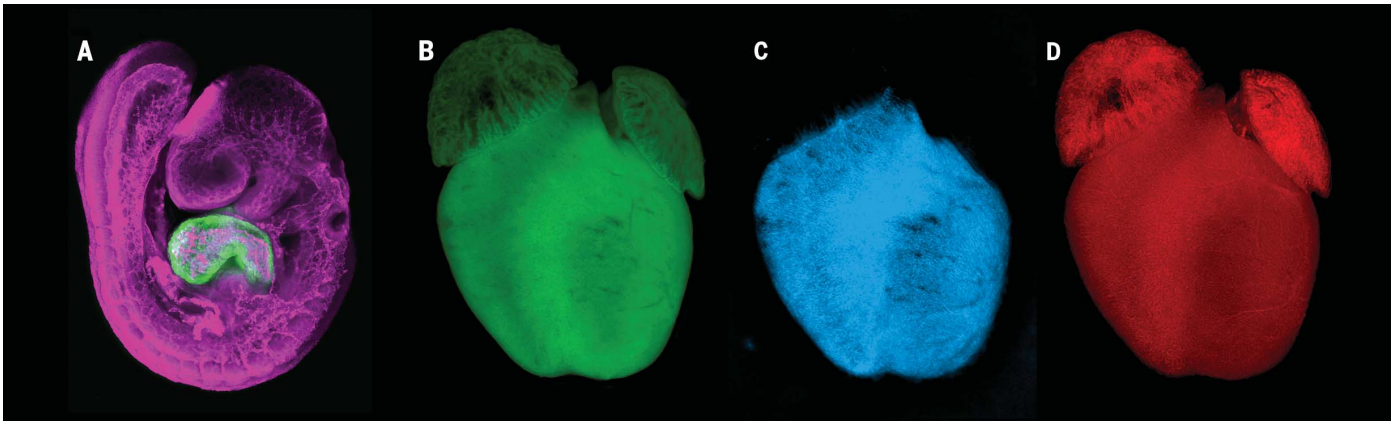


**Monitoring of cell-cell contact in the heart.** (**A**) Whole-mount fluorescence image of a mouse embryo showing that cardiomyocytes and endothelial cells express the synNotch ligand (green) and the synNotch receptor (purple). (**B** to **D**) Whole-mount images of synNotch neonatal hearts shown in green (B), blue (C), and red (D) fluorescence channels. Present and past cell contact signaling are displayed by blue and red fluorescence, respectively.

RESEARCH ARTICLE

SYNTHETIC BIOLOGY

# Monitoring of cell-cell communication and contact history in mammals

Shaohua Zhang[1]†, Huan Zhao[1]†, Zixin Liu[1], Kuo Liu[2], Huan Zhu[1], Wenjuan Pu[1], Lingjuan He[3], Rong A. Wang[4], Bin Zhou[1,2,5]*

**Monitoring of cell-cell communication in multicellular organisms is fundamental to understanding diverse biological processes such as embryogenesis and tumorigenesis. To track cell-cell contacts in vivo, we developed an intercellular genetic technology to monitor cell-cell contact and to trace cell contact histories by permanently marking contacts between cells. In mice, we engineered an artificial Notch ligand into one cell (the sender cell) and an artificial receptor into another cell (the receiver cell). Contact between the sender and receiver cells triggered a synthetic Notch signaling that activated downstream transcriptional programs in the receiver cell, thereby transiently or permanently labeling it. In vivo cell-cell contact was observed during development, tissue homeostasis, and tumor growth. This technology may be useful for studying dynamic in vivo cell-cell contacts and cell fate plasticity.**

Cell-cell communication is ubiquitous in multicellular organisms and is essential in fundamental biological processes, including embryogenesis, immune responses, stem cell fate decisions, and tumorigenesis (*1*–*4*). Technologies that enable monitoring and recording of cell-cell communication have driven advances in our basic understanding of many biological processes (*5*–*12*). For example, intercellular enzymatic proximity labeling has been used to monitor cell-cell communication in vivo and in vitro (*8*, *11*), providing information on immune cell function, and the generation of a cell-penetrating fluorescent protein secreted from tumor cells can be used to label cells in tumor metastatic niches (*13*). However, for long-term tracing of cell contact, existing methods such as tagging of surface proteins or secretion of fluorescent proteins are unsuitable because many cell-cell interactions are dynamic and transient. Existing technologies also cannot monitor and permanently trace dynamic interactions between T cell progenitors and thymus cells before mature T cells migrate to lymphoid organs (*14*), nor can they track transient interactions between tumor cells and their niche cells during dissemination and metastasis (*13*, *15*). Indeed, many biological processes occur weeks or months after (transient) cell-cell contact, such as tumor immune responses and tissue regeneration (*16*–*18*). To understand the dynamics of complex in vivo cell-cell communication over time, we developed a genetic system that converts a cellular contact event into a controllable genetic program, enabling subsequent monitoring of ongoing cell-cell contacts or tracing of cell contact history in vivo (fig. S1). For broader application, we also generated a Cre recombinase–induced genetic tool box that can be used for identifying and manipulating cell lineages directly influenced by cell-cell contact in vivo.

## Results

### *Generation of the gLCCC system for monitoring ongoing cell-cell contacts*

The Notch signaling pathway mediates communication between neighboring cells in many cellular processes during development and homeostasis (*19*, *20*). In the canonical Notch signaling pathway (*21*), binding of the Notch ligand to the Notch receptor triggers γ-secretase–mediated cleavage within the Notch transmembrane region, and the cleaved Notch intracellular domain then translocates into the nucleus and activates the transcription of target genes (Fig. 1A). Like endogenous delta (ligand)–Notch (receptor) communication, activation of a synthetic Notch (synNotch) pathway depends on direct cell-cell contact, which has been used to program contact-dependent transcriptional regulation (*5*–*7*, *10*, *22*, *23*). Given the contact-dependent feature of synNotch activation, we explored its application for in vivo genetic monitoring and tracing of cell-cell contacts. We engineered two separate mouse alleles through gene targeting: One allele encoded a synNotch ligand and the other a synNotch receptor (Fig. 1B). The synNotch ligand is a membrane-tethered green fluorescent protein (mGFP) that serves as an artificial Notch ligand. The synthetic receptor for Notch is a modified Notch protein in which the extracellular and intracellular domains are replaced with a Myc-tagged anti-GFP nanobody (αGFP) and the tetracycline (tet) transactivator (tTA), respectively, which is abbreviated as αGFP-N-tTA (Fig. 1B). To mitigate the potential influence of artificial ligand–receptor binding on dynamic cell-cell interactions such as postcontact dissociation, we used a low-affinity αGFP nanobody (LaG17) that has an affinity for GFP that is 1/70th of that of another αGFP nanobody (LaG16) (*5*, *24*). To target the synNotch ligand to sender cells [e.g., cardiomyocytes (CMs)], mGFP was driven under a CM-specific promoter. To target the synNotch receptor to receiver cells [e.g., endothelial cells (ECs)], αGFP-N-tTA was driven under an EC-specific promoter. In mice carrying both sender and receiver alleles, as well as a reporter allele such as *tetO-LacZ* that encodes the β-galactosidase enzyme for X-galactosidase (X-gal) staining detection (*25*, *26*), if a sender cell contacts a receiver cell, then the binding between GFP and αGFP-N-tTA triggers cleavage of the Notch transmembrane domain, thereby releasing tTA (Fig. 1, C and D). Cleaved tTA then translocates into the nucleus to activate the *tetO-LacZ* reporter system (Fig. 1D). We refer to mice carrying these three genetic elements (synNotch ligand, receptor, and reporter) as gLCCC mice for "genetic labeling of cell-cell contact."

We used CMs as sender cells and ECs as receiver cells (Fig. 1, E and F) and generated cardiac troponin T2 (*Tnnt2*)-*mGFP* knock-in mice to express mGFP specifically in TNNT2$^+$ CMs (Fig. 1E and fig. S2) and cadherin 5 (*Cdh5*)-*αGFP-N-tTA* knock-in mice to express αGFP-N-tTA in CDH5$^+$ ECs (Fig. 1F and fig. S3). Immunostaining and confocal examination of *Tnnt2-mGFP;Cdh5-αGFP-N-tTA* embryos documented the close physical proximity of GFP$^+$ CMs and αGFP$^+$ ECs in the heart (Fig. 1G). We generated *Tnnt2-mGFP;Cdh5-αGFP-N-tTA;tetO-LacZ* (or heart-gLCCC) mice and tested whether contact between sender and receiver cells triggered LacZ expression specifically in cardiac ECs (Fig. 1D). X-gal staining of mouse tissues was used to detect LacZ expression in ECs (*25*, *26*). Although no LacZ-expressing cells were observed in littermate controls with other genotypes, we did observe LacZ expression in the hearts from embryonic day 9.5 (E9.5) heart-gLCCC embryos (Fig. 1H). Immunostaining of sections prepared from these embryos revealed specific LacZ expression in the endocardial ECs located adjacent to GFP$^+$ CMs (Fig. 1, I and J). To confirm that LacZ expression was specifically triggered by the synNotch pathway, we showed that heart-gLCCC embryos exposed to the γ-secretase

[1]State Key Laboratory of Cell Biology, CAS Center for Excellence in Molecular Cell Science, Shanghai Institute of Biochemistry and Cell Biology, Chinese Academy of Sciences, University of Chinese Academy of Sciences, Shanghai 200031, China. [2]Key Laboratory of Systems Health Science of Zhejiang Province, School of Life Science, Hangzhou Institute for Advanced Study, University of Chinese Academy of Sciences, Hangzhou 310024, China. [3]School of Life Sciences, Westlake University, Hangzhou, Zhejiang 310030, China. [4]Laboratory for Accelerated Vascular Research, Department of Surgery, Division of Vascular Surgery, University of California, San Francisco, CA 94143, USA. [5]School of Life Science and Technology, ShanghaiTech University, Shanghai 201210, China.
*Corresponding author. Email: zhoubin@sibs.ac.cn
†These authors contributed equally to this work.

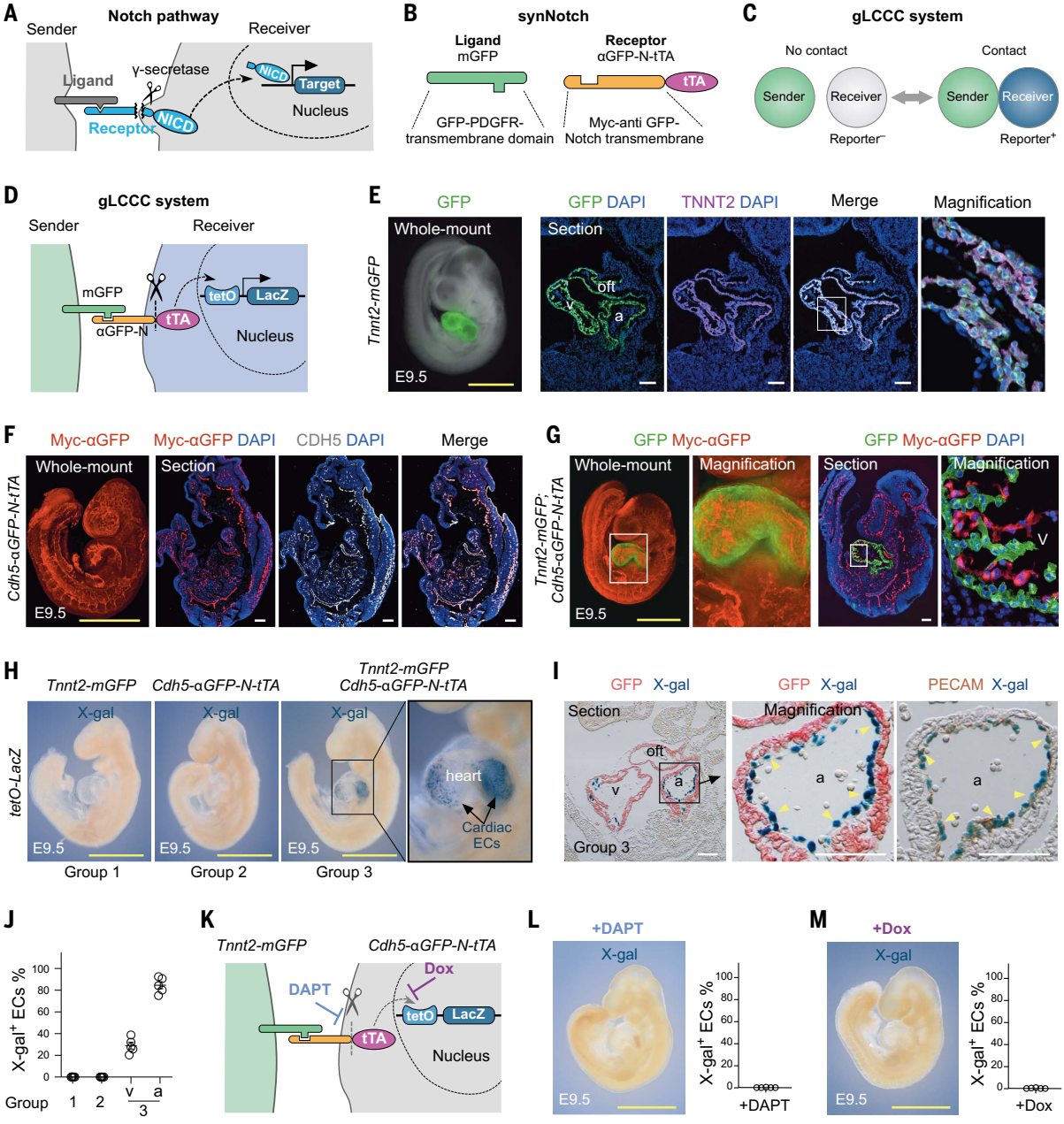


**Fig. 1. Genetic labeling of in vivo cell-cell contact.** (**A**) Schematic figure showing the canonical Notch signaling pathway. NICD, Notch intracellular domain. (**B**) Schematic showing components of the synNotch pathway: mGFP as ligand and αGFP-N-tTA as receptor. αGFP is myc-tagged. (**C**) Illustration showing the gLCCC system for genetic labeling of cell-cell contact. (**D**) Schematic showing the overall design of the gLCCC system. Binding of GFP to the αGFP nanobody leads to cleavage of the transmembrane domain of the synNotch receptor by γ-secretase. This subsequently releases tTA, which then translocates into the nucleus and activates LacZ expression. (**E** to **G**) Whole-mount and sectional immunostaining images of E9.5 *Tnnt2-mGFP* (E), *Cdh5-αGFP-N-tTA* (F), and *Tnnt2-mGFP;Cdh5-αGFP-N-tTA* (G) embryos. (**H**) Whole-mount X-gal staining for the detection of the β-galactosidase enzyme encoded by the LacZ gene on E9.5 *Tnnt2-mGFP;tetO-LacZ* (group 1), *Cdh5-αGFP-N-tTA;tetO-LacZ* (group 2), and *Tnnt2-mGFP;Cdh5-αGFP-N-tTA;tetO-LacZ* (group 3) embryos. Arrows indicate LacZ$^+$ cardiac ECs. (**I**) X-gal staining with immunostaining of *Tnnt2-mGFP;Cdh5-αGFP-N-tTA;tetO-LacZ* embryonic sections for GFP or PECAM. Arrowheads indicate LacZ$^+$ cardiac ECs. (**J**) Quantification of the percentage of LacZ$^+$ ECs in embryos of different genotypes. Data are shown as the mean ± SEM; $n$ = 5. v, ventricle; a, atrium. (**K**) Schematic showing inhibition of γ-secretase activity by DAPT or inhibition of tTA binding to tetO by Dox. (**L** and **M**) Whole-mount X-gal staining on *Tnnt2-mGFP;Cdh5-αGFP-N-tTA;tetO-LacZ* embryos after DAPT (L) or Dox (M) treatment. Right panel shows the quantification of the percentage of LacZ$^+$ ECs. Data are shown as the mean ± SEM; $n$ = 5. Scale bars: yellow, 1 mm; white, 100 μm. Each image is representative of five individual biological samples.

inhibitor *N*-[*N*-(3,5-difluorophenacetyl)-l-alanyl]-S-phenylglycine t-butyl ester (DAPT) (*27*) had no LacZ$^+$ cells (Fig. 1, K and L). To validate Tet-responsive expression, we showed that heart-gLCCC embryos exposed to doxycycline (Dox), which inactivates tTA (*28*), had no LacZ$^+$ cells (Fig. 1, K to M). We also used *Tnnt2-mGFP;Cdh5-αGFP-N-tTA;tetO-tdT* (where tdT is tdTomato) mice to further validate the dynamic contacts between ECs and CMs in postnatal hearts (fig. S4). Thus, this gLCCC system offers cell contact–specific labeling of ECs in contact with CMs.

To determine how long cell-cell contact is needed to activate the gLCCC system, we cultured sender and receiver cells in vitro and found by fluorescence microscopy that tdT$^+$ cells started to appear after 4 hours of contact (fig. S5, A to D). Alternatively, we used DAPT to inhibit the gLCCC system at different time points and assessed tdT expression after 36 hours of co-culture. Within 2 hours of cell-cell contact, we detected receiver cells expressing tdT (fig. S5, E to H). Free mGFP protein did not lead to tdT expression in receiver cells (fig. S6). Half of cardiac ECs lost tdT 2 days after inhibition of contact-activated gLCCC (fig. S7).

To test whether cardiac ECs continue to interact with surrounding CMs in the adult heart, we collected hearts from 12-week-old *Tnnt2-mGFP;Cdh5-αGFP-N-tTA;tetO-tdT* mice (fig. S8, A and B). Immunostaining of heart sections for GFP, tdT, and CDH5 showed that a proportion of coronary capillary ECs expressed tdT (fig. S8, C and D), suggesting that they were in contact with CMs. Transmission electron microscopy of adult wild-type hearts provided morphological evidence showing the close proximity between the plasma membranes of CMs and ECs (fig. S8, E and F). One advantage of the tdT reporter is that it enables the isolation of cells by flow cytometry for further characterization of ECs that had contact with CMs. Isolated tdT$^+$ ECs showed increased expression of genes for cellular respiration, intrinsic apoptotic signaling, and cellular responses to stress (fig. S8, G to K). In addition to heart-gLCCC, we also generated liver-gLCCC with hepatocyte-specific promoter albumin-driven mGFP (*Alb-mGFP*) mice and *Cdh5-αGFP-N-tTA;tetO-tdT* mice and found that EC-hepatocyte contact activated tdT expression in postnatal day 0 (P0) livers (fig. S9) but not in adult livers (fig. S10). This suggested that gLCCC could be used to study dynamic cell-cell contacts in multiple cell types.

### Generation of a gTCCC system for genetic tracing of cell-cell contact history

To enable tracking of receiver cells that had any history of contact with sender cells, we incorporated the Cre-loxP system downstream of the synNotch pathway (Fig. 2A). The tTA reporter was replaced by *tetO-Cre* and a Rosa26 (R26)-floxed-Stop-reporter, which is located in the ubiquitously active gene locus Rosa26 (*29*). Sender-receiver cell contact triggered activation of the synNotch pathway and translocation of tTA into the nucleus, turning on the expression of Cre recombinase in the receiver. Cre then mediated irreversible Cre-loxP recombination, leading to constitutive expression of tdT in the receiver and all of its descendants, thus permanently tagging them (Fig. 2A), even if the receiver no longer had contact with the sender or its descendants had never contacted any sender. Therefore, any contact event would genetically tag the receiver cell, allowing genetic tracing of such receiver cells and their progenies even after they migrated away from the sender cells or differentiated or transformed into other cell lineages. We call mice carrying synNotch and Cre-loxP systems gTCCC mice for "genetic tracing of cell-cell contact."

We studied migration and fate transitions of endocardial ECs in the developing mouse heart. Cardiac ECs contact CMs during early embryonic heart development (*30*). In cardiac valve formation, these endocardial ECs then shift to a mesenchymal fate and migrate into the cardiac cushion through the endothelial-to-mesenchymal transition (EMT) program (*30*) (Fig. 2B). In mice, this dissociation of endocardial ECs away from CMs is already completed before P0, when the cardiac cushion has been remodeled into cardiac valves and mesenchymal cells in the valve no longer express any EC markers (Fig. 2B). We generated *Tnnt2-mGFP;Cdh5-αGFP-N-tTA;tetO-Cre;R26-tdT* or heart-gTCCC mice (Fig. 2A). The tdT signals that we observed in heart-gTCCC mice at E9.0 indicated that the cardiac ECs were successfully genetically labeled, and their mesenchymal descendants maintained tdT expression at E10.0 (Fig. 2, C and D). These data demonstrated that the genetic tracer tdT was permanently maintained in the receiver cells and all of their descendants, even when their descendants changed cell fate, e.g., due to EMT during cardiac valve development.

Whole-mount fluorescence images of organs, immunostaining of tissue sections, and flow cytometric analysis revealed that most of the cardiac ECs retained tdT expression in the heart-gTCCC mice at P0, whereas no tdT expression was observed in their littermate controls of other genotypes (Fig. 2, E to H). We rarely detected tdT$^+$ ECs in other heart-gTCCC mouse organs examined, with the exception of the liver (see below) (fig. S11). Dox administration abolished tdT labeling of cardiac ECs in heart-gTCCC mice, demonstrating controllable genetic regulation by the Tet system (Fig. 2, E to H). At P0, even though the descendants of ECs that became mesenchymal cells in the valve were nowhere near CMs, they maintained tdT expression (Fig. 2I), which verified their EMT fate transition. These tdT$^+$ valve interstitial cells expressed mesenchymal cell marker platelet–derived growth factor receptor α (PDGFRα) (Fig. 2I), but they no longer expressed the EC marker platelet EC adhesion molecule (PECAM) (Fig. 2I). Thus, we could trace ECs even after they switched fate to mesenchymal cells.

Endocardial ECs migrate at E8.5 to the nearby liver bud, where they contribute to the liver vasculature (*31*) (Fig. 2J). We found that a subset of ECs in postnatal liver had contact with CMs at an early embryonic stage. About 20% of ECs in livers collected from P0 heart-gTCCC mice showed tdT fluorescence (Fig. 2, K and L, and fig. S11B). We did not detect any tdT$^+$ ECs in the livers collected from P0 *Cdh5-αGFP-N-tTA;tetO-Cre;R26-tdT* littermate controls (Fig. 2K). Considering that no liver cells expressed mGFP synNotch ligand in the heart-gTCCC mice (fig. S11B), the tdT$^+$ ECs in the liver at P0 likely originated from the heart (*31*), and these ECs probably contacted mGFP$^+$ CMs before their migration into the liver bud (Fig. 2J). Furthermore, these tdT$^+$ ECs were maintained in the adult liver, where they may contribute to the adult liver vasculature (fig. S12, A to D). We therefore were able to detect cell-cell communication temporally and spatially isolated during organogenesis and homeostasis (fig. S12, E and F).

### Genetic tracing of cell-cell contact history reveals outgrowth of tumor angiogenesis

To further demonstrate the utility of gTCCC for tracing cell contact histories, we studied vascular ECs in tumor angiogenesis, during which blood vessels are recruited from peripheral tissues into hypoxic tumors (*32*–*34*). In this pathological condition, ECs migrate into tumors, and their contact history with tumor cells may confer them with particular capabilities of tumor blood vessels (*34*). We traced ECs that had contact with tumor cells and followed EC fate during tumor growth in vivo. The mouse lung tumor cell line TC-1 was engineered to constitutively express mGFP (TC-1-mGFP) as sender cells, and these cells were in direct contact with infiltrating ECs from host mice (fig. S13). To genetically trace tumor-infiltrating ECs, we implanted TC-1-mGFP tumor cells into *Cdh5-αGFP-N-tTA;tetO-Cre;R26-tdT* receiver mice (Fig. 3A) and collected tissues for analysis 7 and 14 days after implantation (Fig. 3B). ECs showed tdT fluorescence in TC-1-mGFP tumors at day 7 (Fig. 3, C and D), but not in TC-1 control tumors (Fig. 3, C and D) or other organs at any stage analyzed in *Cdh5-αGFP-N-tTA;tetO-Cre;R26-tdT* mice (fig. S14). *Bandeiraea simplicifolia* lectin injection showed that these tdT$^+$ ECs were functionally connected to circulation (Fig. 3E). These tdT$^+$ ECs were mainly found in tumors, not in the thin layer of peripheral capsule tissue, at day 7 (Fig. 3, F and G).

At day 14, however, we observed tdT$^+$ ECs outside of the tumor, in the peripheral capsule tissues that were free of any mGFP$^+$ tumor cells (Fig. 3, H and I). The thick layer of capsule detected at day 14 was enriched in fibroblasts and macrophages (Fig. 3J), which may produce angiogenesis factors to recruit ECs from within tumors. Indeed, we detected enriched vascular endothelial growth factor A (VEGFA) expression in the thick peripheral capsule at day 14 (Fig. 3J), which may partly explain the strong recruitment of blood vessels by the tumor. We used Dox treatment to inhibit the gTCCC system at different times after

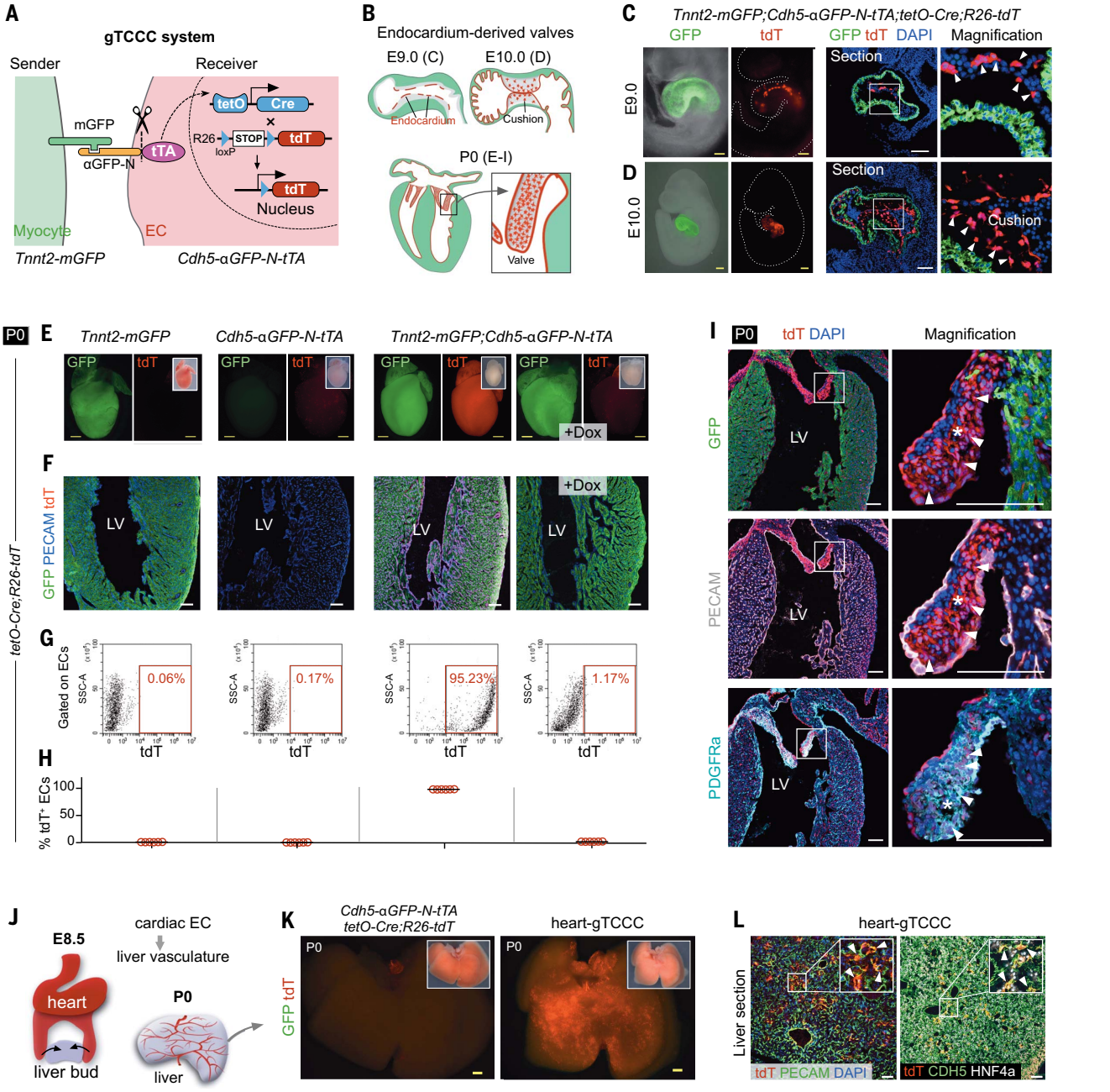


**Fig. 2. Genetic tracing of ECs that have had contact with CMs.** (**A**) Schematic showing the gTCCC strategy for permanent genetic tracing of cardiac ECs that have had contact with CMs. (**B**) Illustration of the development of the endocardial cushion and cardiac valves (red). Green indicates CMs. (**C** and **D**) Whole-mount fluorescence images of E9.0 (C) and E10.0 (D) *Tnnt2-mGFP;Cdh5-αGFP-N-tTA;tetO-Cre;R26-tdT* (heart-gTCCC) embryos and immunostaining for tdT and GFP. (**E**) Whole-mount fluorescence images of P0 hearts collected from mice of different genotypes as indicated. Inserts are bright-field images. Dox was added to inhibit the Tet system. (**F**) Immunostaining of heart sections for GFP, tdT, and PECAM. (**G**) Fluorescence-activated cell sorting (FACS) analysis of tdT$^+$ cardiac ECs from hearts. (**H**) Quantification of the percentage of ECs expressing tdT. Data are shown as the mean ± SEM; $n$ = 6. (**I**) Immunostaining of heart sections for tdT and GFP, PECAM, or PDGFR$\alpha$. Arrowheads indicate tdT$^+$ mesenchymal cells in valves (asterisks). (**J**) Illustration showing that ECs from the developing heart migrate to the liver bud at E8.5 and subsequently contribute to the liver vasculature. (**K**) Whole-mount fluorescence images of P0 livers. (**L**) Immunostaining of P0 liver sections for tdT and PECAM or tdT, CDH5, and HNF4a. Arrowheads indicate tdT$^+$ ECs. Scale bars: yellow, 400 μm; white, 100 μm. Each image is representative of six individual biological samples. Data are shown as mean ± SEM.

tumor implantation and found that tumor-infiltrating ECs at early stages (i.e., the first 5 days) were genetically labeled and subsequently moved to the tumor capsule (fig. S15). Thus, the ability of our gTCCC system to trace the postcontact history of cells throughout their lifetimes enabled us to show that some vascular ECs, after dissociating from cancer cells, extended into the peripheral tissues with no tumor cells (Fig. 3K).

We sorted three types of ECs from implanted tumors: tdT$^+$ tumor ECs (tdT$^+$ tECs), tdT$^+$ capsule ECs (tdT$^+$ cECs), and cECs lacking tdT fluorescence (tdT$^-$ cECs) (Fig. 3L). Principal component analysis revealed three

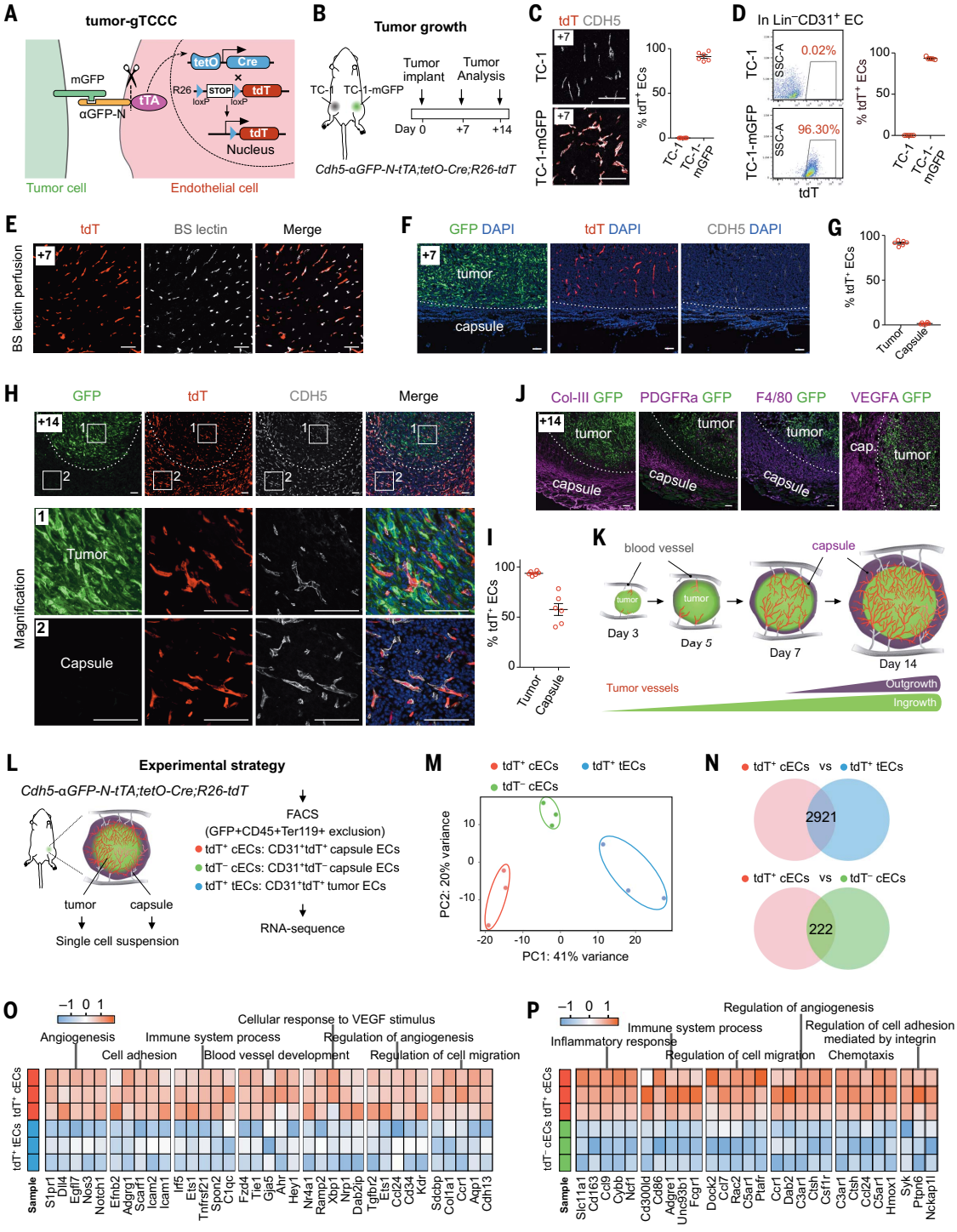


**Fig. 3. Genetic tracing of the tumor cell–EC interaction during tumor growth.** (**A** and **B**) Schematic showing the tumor-gTCCC strategy to trace tumor cell–EC contact history (A) and experimental design (B). (**C**) Immunostaining of tumor sections 7 days after tumor implantation (+7 day). Right panel shows quantification data for the percentage of ECs expressing tdT. (**D**) FACS analysis of the percentage of $CD31^+$ ECs expressing tdT in +7 day tumors. (**E**) Detection of perfused *Bandeiraea simplicifolia* lectin in tumor $tdT^+$ ECs showing functional blood vessels in tumors. (**F** and **H**) Immunostaining of tumor sections of +7 day (F) and +14 day (H) tumors for GFP, tdT, and CDH5. (**G** and **I**) Quantification of the percentage of ECs expressing tdT in the tumor or capsule at +7 (G) and +14 (I) days. (**J**) Immunostaining of +14 day tumor sections for fibroblast and macrophage markers. (**K**) Illustration showing that vessels expand from the periphery into the tumor (ingrowth) and $tdT^+$ vessels expand out of the tumor into the peripheral capsule (outgrowth) during tumor growth and formation of the capsule. (**L**) Schematic diagrams illustrating the experimental strategy for RNA-sequencing experiments. (**M**) Principal component analysis of $GFP^-CD45^-Ter119^-CD31^+$ cell signatures from tECs and cECs. $n = 3$. (**N**) Venn diagram of differentially expressed gene numbers in the $tdT^+$ cEC versus $tdT^+$ tEC group and in the $tdT^+$ cEC versus $tdT^-$ cEC group. (**O** and **P**) Heatmap generated from the top differentially expressed genes in the enriched pathways. Scale bars, 100 μm. Data are shown as mean ± SEM. Each staining is representative of six individual biological samples.

different groups of ECs with distinct transcriptional profiles (Fig. 3M). Comparisons of gene expression between tdT$^+$ cECs and tdT$^+$ tECs highlighted enriched pathways for angiogenesis, cell adhesion, the immune system process, blood vessel development, cellular response to VEGF stimulus, and regulation of cell migration in tdT$^+$ cECs compared with those from tdT$^+$ tECs (Fig. 3, N and O, and fig. S16A). Comparison of gene expression between tdT$^+$ cECs and tdT$^-$ cECs showed increased expression of genes associated with inflammatory responses, immune system processes, positive regulation of cell migration and angiogenesis, chemotaxis, and regulation of cell adhesion in tdT$^+$ cECs versus tdT$^-$ cECs. This suggested that an interaction between ECs and tumor cells may endow these ECs with particular properties in angiogenesis, migration, and the inflammatory response (Fig. 3P and fig. S16B). It appears possible that blood vessels, when recruited into tumors, can grow out of tumors into peripheral capsules.

### *Cre-induced R26-mGFP* mouse line for broad spectrum of cell types as sender cells

To broaden the application of the gLCCC and gTCCC systems to all cell types that contact a particular receiver cell type, we generated a knock-in mouse line, *R26-mGFP*, for Cre-dependent expression of mGFP ligand in sender cells (Fig. 4A). We inserted an mGFP transgene expression cassette into the ubiquitous *Rosa26* locus, with the mGFP coding sequences following a loxP-flanked 3x polyA Stop cassette to render mGFP expression inducible upon Cre recombinase administration (Fig. 4A). Whole-mount fluorescence or sectional staining of E15.5 *R26-mGFP* embryos showed no GFP expression (Fig. 4B), indicating no leakiness of GFP expression without Cre recombinase. By contrast, *ACTB-Cre;R26-mGFP* embryos, which had Cre-loxP–mediated excision in all cells, yielded GFP expression throughout (Fig. 4C), demonstrating that mGFP synNotch ligand expression in targeted cells was Cre dependent.

To use *R26-mGFP* mice to study any other Cre$^+$ cell–EC contacts, we crossed them with *Nestin-CreER*, an inducible Cre driver in Nestin$^+$ cells that include neurons, epididymis vascular smooth mucle cells, and myoblasts. We generated *Nestin-CreER;R26-mGFP* senders and *Cdh5-αGFP-N-tTA;tetO-tdT* receiver or Nestin-gLCCC mice (Fig. 4D). We treated the Nestin-gLCCC mice with tamoxifen (Tam) at E12.5 to induce Cre activation and found, at E15.5, that some GFP$^+$ cells expressed the neuronal nuclear protein (NeuN), and they were in proximity with cadherin 5–positive (CDH5$^+$) ECs (Fig. 4, E to F). Fluorescence imaging of sagittal sections of E15.5 embryos showed that tdT signals mirrored the GFP expression pattern, except in the brain, where there was no detectable tdT expression (Fig. 4G). The tdT$^+$ ECs were located in the trigeminal ganglion, dorsal root ganglion, and intercostal neurovascular bundle, but there were no tdT$^+$ ECs detected in the brain (Fig. 4H and fig. S17). In mice of the same genotype treated with corn oil (designated the "no Tam" group), neurons did not express GFP and ECs remained tdT$^-$ in the trigeminal ganglion (Fig. 4I). We confirmed that tdT expression in ECs was controlled by the tet-regulated genetic system, because Dox administration repressed tdT expression in ECs of Tam-treated Nestin-gLCCC mice (Fig. 4J). Therefore, *R26-mGFP* is applicable for generating sender cells from any Cre-expressing cell type (Fig. 4K).

### *Cre-induced H11-αGFP-N-tTA* mouse line enabling any cell type to be receiver cells

To find all of the cell types that interact with a particular sender cell, we generated a knock-in mouse line, *H11-αGFP-N-tTA*, for Cre-dependent expression of the αGFP-N-tTA receptor in receiver cells (Fig. 5A). We then inserted an αGFP-N-tTA expression cassette into another ubiquitous gene locus, *Hipp11* (*35*), with the αGFP-N-tTA coding sequences following a loxP-flanked 3x polyA stop cassette to render receptor expression inducible upon Cre recombinase administration (Fig. 5A). Sectional staining of E15.5 *H11-αGFP-N-tTA* embryos showed no Myc-αGFP (annotation of αGFP-N-tTA) expression (Fig. 5B), indicating no receptor expression without Cre recombinase. By contrast, *Tie2-Cre;H11-αGFP-N-tTA* embryos, with Cre-loxP–mediated excision in all endothelial lineages, yielded receptor expression throughout (Fig. 5, C and D), demonstrating that αGFP-N-tTA synNotch receptor expression in targeted cells was Cre dependent.

To functionally characterize *H11-αGFP-N-tTA* mice in studying cell-cell interactions, we crossed *Tnnt2-mGFP* mice with *Tie2-Cre;H11-αGFP-N-tTA* mice and used *tetO-tdT* as the readout of their contacts (Fig. 5E). In *Tnnt2-mGFP;H11-αGFP-N-tTA;tetO-tdT* mice, we could not detect tdT expression in the heart unless the mice were crossed with the *Tie2-Cre* mouse line (Fig. 5F). Immunostaining of heart sections of *Tnnt2-mGFP;Tie2-Cre;H11-αGFP-N-tTA;tetO-tdT* mice for GFP and tdT showed tdT expression in a vascular pattern (Fig. 5G). Most of the ECs in the atrium and ventricle were tdT$^+$, except for endocardial ECs on the valves, where they were anatomically separated from CMs (Fig. 5H). No tdT$^+$ ECs were detected in other organs or tissues (Fig. 5I), indicating that the genetic activity of receptor-expressing cells also depends on ligand from sender cells, e.g., mGFP$^+$ CMs. Therefore, *H11-αGFP-N-tTA* is applicable for generating receiver cells from any Cre-expressing cell type (Fig. 5J).

### *One Tigre-synNotch* mouse allele to unravel any cells that contact Cre$^+$ cells

To facilitate the broad application of an intercellular genetic approach, we generated a Cre-induced synNotch allele on the tightly regulated (Tigre) genomic locus (*36*), resulting in a *Tigre-synNotch* mouse that could simultaneously express synthetic ligand in Cre$^+$ cell lineages and receptor in Cre$^-$ cells. In this *Tigre-synNotch* design, tetO-rox-Stop-rox-tdT-insulator-CAG-loxP-αGFP-N-tTA-pA-loxP-mGFP was knocked into the *Tigre* gene locus by CRISPR-Cas9 such that the receptor, ligand, and tTA readouts were all combined in one mouse allele (Fig. 6A). By crossing this *Tigre-synNotch* mouse with any Cre mouse, Cre-loxP recombination would remove the loxP-flanked αGFP-N-tTA cassette, leading to mGFP ligand expression in Cre$^+$ sender cells, whereas Cre$^-$ cells continued to express αGFP-N-tTA receptor as receivers (Fig. 6B). *CAG-Dre* was used to remove rox-Stop-rox in *Tigre-synNotch* allele (Fig. 6B). If any Cre$^-$ cells were in contact with Cre$^+$ cells, then tTA would activate tdT in these αGFP-N-tTA$^+$ receiver cells (Fig. 6B). The generation of *Tigre-synNotch* facilitated the genetic detection of in vivo cell-cell contacts using a single Cre-responsive mouse allele.

To test this *Tigre-synNotch* allele, we crossed it with the TEK receptor tyrosine kinase (*Tie2*)–*Cre* line (*37*) and collected *Tie2-Cre;CAG-Dre;Tigre-synNotch* mouse tissues for analysis. Compared with littermate control *CAG-Dre;Tigre-synNotch*, we could detect patterning of tdT robustly in *Tie2-Cre;CAG-Dre;Tigre-synNotch* mice (Fig. 6C). Immunostaining of *Tie2-Cre;CAG-Dre;Tigre-synNotch* mouse tissues such as heart and lung for GFP and PECAM revealed GFP expression in PECAM$^+$ ECs (Fig. 6D). Immunostaining of tissue sections for GFP and tdT showed a particular patterning of tdT that lined along GFP$^+$ cells throughout different organs or tissues (Fig. 6E). For example, these GFP$^+$ ECs contacted PDGFRβ$^+$ pericytes in the brain, TNNT2$^+$ CMs in the heart, PDGFRα$^+$ fibroblasts in the lung, and hepatocytes in the liver, marking these diverse types of cells as tdT$^+$ (Fig. 6F). By contrast, we detected very few tdT$^+$ cells in *CAG-Dre;Tigre-synNotch* mouse tissues (Fig. 6G). Additionally, we used inducible Cre lines to label their neighboring cells as tdT$^+$. For instance, after induction with a low dose of Tam, *Nestin-CreER*– or *CAG-CreER*–labeled sparse mGFP$^+$ cells activated tdT expression only in their neighboring cells (Fig. 6H and fig. S18). These results demonstrated that *Tigre-synNotch* enables the detection of in vivo cell-cell contacts broadly in any given cell type in a Cre mouse line (Fig. 6I).

### *Simultaneous application of gLCCC and gTCCC in one mouse*

To enable the simultaneous detection of ongoing cell-cell contact and contact history in

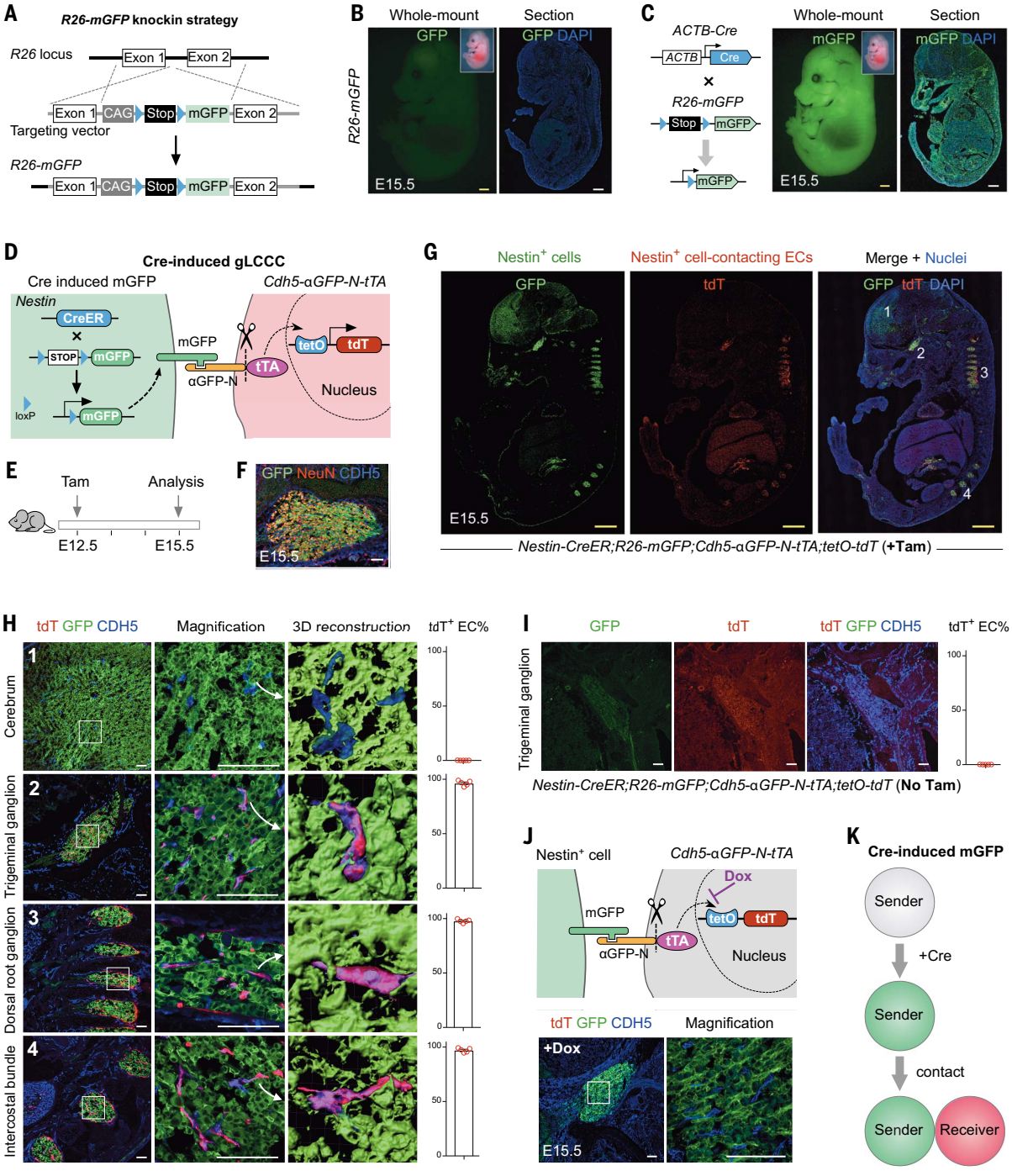


**Fig. 4. Generation of the *R26-mGFP* mouse line for Cre-induced mGFP in sender cells.** (**A**) Schematic showing the generation of the *R26-mGFP* allele by homologous recombination using CRISPR-Cas9. (**B**) Whole-mount or sectional fluorescence images of E15.5 *R26-mGFP* embryos. Insert, bright-field whole-mount image. (**C**) Whole-mount or sectional fluorescence images of E15.5 *ACTB-Cre;R26-mGFP* embryos. Insert, bright-field whole-mount image. (**D**) Schematic showing the design of the Cre-induced gLCCC system for study of the interaction between Cre$^+$ cells and receiver cells, e.g., the Nestin$^+$ cell–EC interaction. (**E**) Schematic showing the experimental design by Tam induction of Cre (*Nestin-CreER*). (**F**) Immunostaining of an E15.5 tissue section for GFP, NeuN, and CDH5 showing that GFP is specifically expressed in neurons. (**G**) Immunostaining of E15.5 whole embryonic sections for GFP and tdT. Regions 1 to 4 are magnified in (H). (**H**) Immunostaining of E15.5 tissue sections for GFP, tdT, and CDH5. Three-dimensionally reconstructed images show neurons (GFP) and their interacting ECs (tdT). The percentage of ECs expressing tdT in each region is quantified on the right panels. Data are shown as the mean ± SEM; $n = 5$. (**I**) Immunostaining of E15.5 embryonic sections from mice that received no Tam for GFP, tdT, and CDH5. Quantification data are shown in the right panel. Data are shown as the mean ± SEM; $n = 5$. (**J**) Dox treatment inhibits tTA binding to tetO, preventing tdT gene activation. Shown is immunostaining of E15.5 tissue sections from the trigeminal ganglion for tdT, GFP, and CDH5 in *Nestin-CreER;R26-mGFP;Cdh5-αGFP-N-tTA;tetO-tdT* mice treated with Dox and Tam. (**K**) Illustration showing Cre-induced mGFP expression in sender cells. Scale bars: yellow, 1 mm; white, 100 μm. Each image is representative of five individual biological samples.

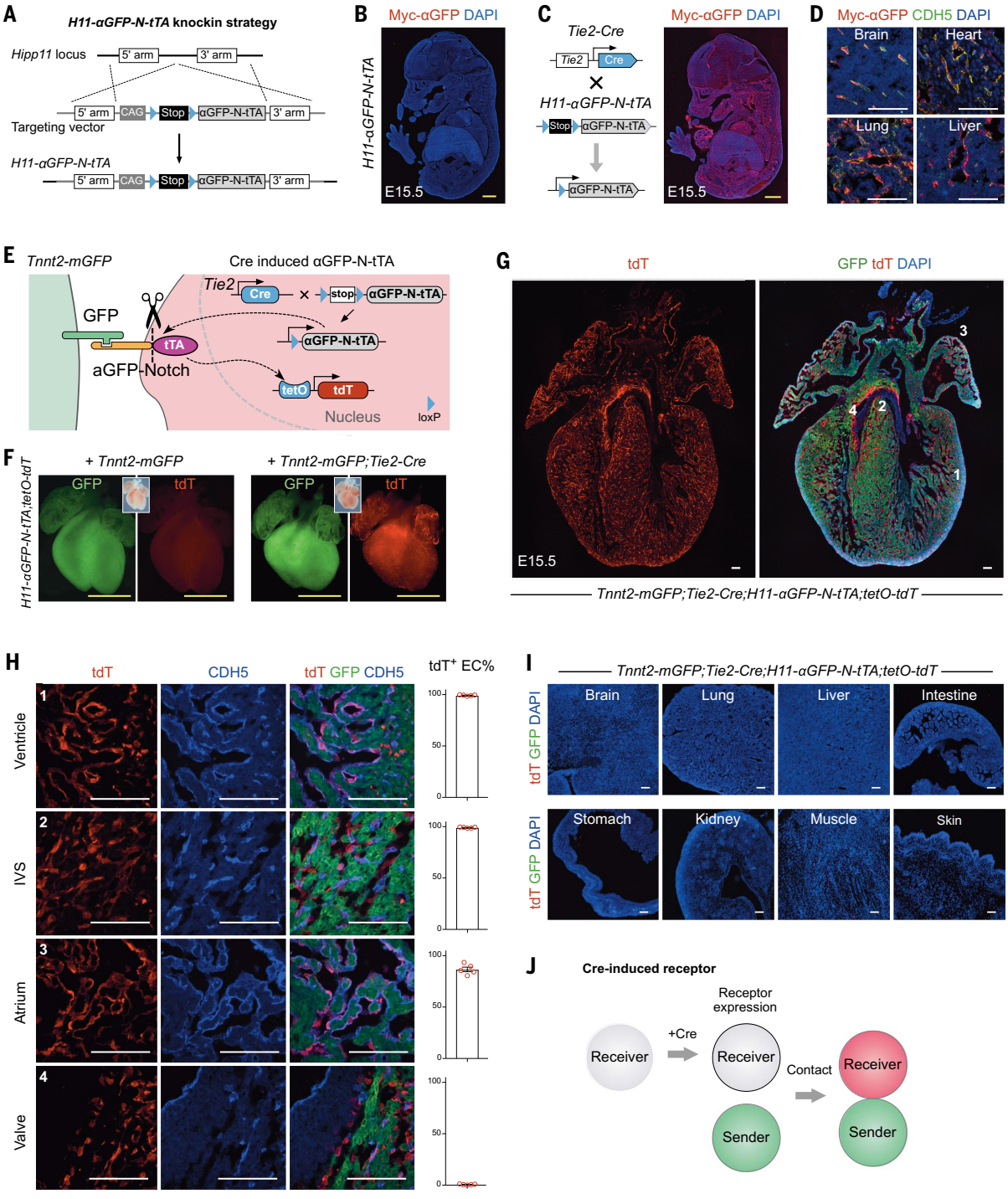


**Fig. 5. Generation of the *H11-αGFP-N-tTA* mouse line for Cre-induced αGFP-N-tTA in receiver cells.** (**A**) Schematic showing the generation of the *H11-αGFP-N-tTA* allele by homologous recombination using CRISPR-Cas9. (**B**) Immunostaining of *H11-αGFP-N-tTA* embryonic sections for the Myc tag. (**C**) Schematic showing *Tie2-Cre*–induced αGFP-N-tTA expression (left). Shown is immunostaining of *Tie2-Cre;H11-αGFP-N-tTA* sections (right) for the Myc tag. (**D**) Immunostaining of brain, heart, lung, and liver sections from E15.5 *Tie2-Cre; H11-αGFP-N-tTA* embryos for the Myc tag and CDH5. (**E**) Schematic showing the design of the Cre-induced gLCCC system for study of the interaction between sender and Cre$^+$ receiver, e.g., the CM-EC interaction. (**F**) Whole-mount fluorescence images of hearts from E15.5 embryos. Insert, bright-field whole-mount images. (**G** and **H**) Immunostaining of E15.5 heart sections for GFP and tdT (G). Regions 1 to 4 are magnified in (H). The percentage of ECs expressing tdT in each region is quantified on the right panels. Data are shown as the mean ± SEM; $n = 5$. (**I**) Immunostaining of other tissues of E15.5 embryos for GFP and tdT. (**J**) Illustration showing Cre-induced αGFP-N-tTA expression in receiver cells. Scale bar: yellow, 1 mm; white, 100 μm. Each image is representative of five individual biological samples.

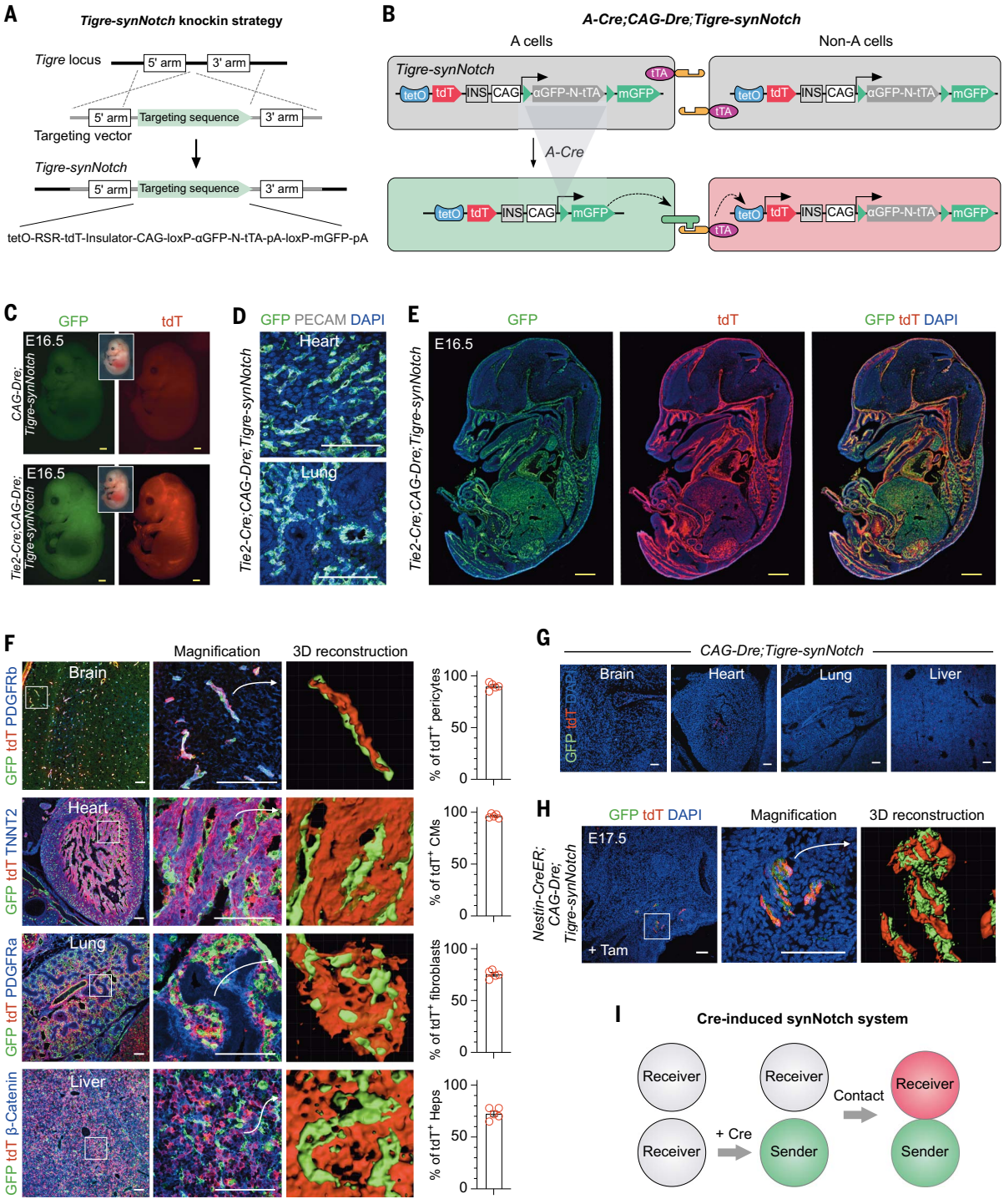


**Fig. 6. Generation of the *Tigre-synNotch* mouse line for labeling of cells that contact with any Cre$^+$ cells.** (**A**) Schematic showing the generation of the *Tigre-synNotch* allele by homologous recombination using CRISPR-Cas9. (**B**) Schematic showing the design for labeling of cells that contact with any Cre$^+$ cell lineages. (**C**) Whole-mount fluorescence images of E16.5 *CAG-Dre; Tigre-synNotch* and *Tie2-Cre;CAG-Dre;Tigre-synNotch* embryos. Insert, bright-field whole-mount image. (**D**) Immunostaining of E16.5 sections from *Tie2-Cre;CAG-Dre; Tigre-synNotch* embryos for GFP and PECAM. (**E**) Immunostaining of E16.5 whole embryonic sections from *Tie2-Cre;CAG-Dre;Tigre-synNotch* for GFP and tdT. (**F**) Immunostaining of E16.5 tissue sections for GFP, tdT, and PDGFRb, TNNT2, PDGFRα, or β-catenin. Three-dimensionally reconstructed images show GFP$^+$ cells and their interacting tdT$^+$ cells. The percentage of pericytes, CMs, fibroblasts, and hepatocytes expressing tdT in each region is quantified in the right panels. Data are shown as the mean ± SEM; $n = 5$. (**G**) Immunostaining of E16.5 sections from *CAG-Dre;Tigre-synNotch* embryos for GFP and tdT. (**H**) Immunostaining of E17.5 embryonic sections from *Nestin-CreER;CAG-Dre;Tigre-synNotch* for GFP and tdT after a low dose of Tam at E12.5. (**I**) Illustration showing the process of the Cre-induced synNotch system for labeling cells that contact with any Cre$^+$ cell lineage. Scale bars: yellow, 1 mm; white, 100 μm. Each image is representative of five individual biological samples. Data are shown as mean ± SEM.

one mouse, we generated a *tetO-Dre-BFP* reporter line [where Dre is another site-specific recombinase targeting specific 32bp DNA site rox (*38*), and BFP is blue fluorescent protein], by which an insulator-flanked tetO-Dre-IRES-BFP-polyA cassette was knocked into the Rosa26 locus using CRISPR-Cas9 (fig. S19A). In this design, when a mGFP$^+$ receiver cell and an αGFP-N-tTA$^+$ sender cell come into contact, tTA activates Dre-BFP expression, marking receiver cells as BFP$^+$ (gLCCC; fig. S19B). Using *R26-rox-tdT* (Rosa26-rox-Stop-rox-tdTomato), Dre-rox recombination results in permanent genetic tracing of receiver cells by tdT (gTCCC; fig. S19B). We used cardiac EC-CM contact to test this simultaneous gLCCC and gTCCC system using *Tnnt2-mGFP;Cdh5-αGFP-N-tTA;tetO-Dre-BFP;R26-rox-tdT* mice. Using whole-mount fluorescence and sectional immunostaining, we found that BFP and tdT were both expressed in CDH5$^+$ ECs in the heart (fig. S19, C and D). In mice lacking either synthetic ligand or receptor, we did not detect any BFP or tdT in cardiac ECs (fig. S19, C and D), suggesting that simultaneous gLCCC and gTCCC activation requires contact with both the synNotch ligand and the synNotch receptor.

We next used BFP (for gLCCC) and tdT (for gTCCC) to distinguish ongoing cell-cell contact and contact history in one mouse. Considering the established models of endocardial EMT in valve formation (*30*) and endocardial contribution to the liver vasculature (*31*), we examined BFP and tdT reporter in valve mesenchymal cells and ECs in the liver. Immunostaining of heart and liver sections showed that tdT was still expressed in valve mesenchymal cells and liver ECs when they were no longer in contact with GFP$^+$ CMs, but they did not express any BFP (fig. S19, E and F). Coronary ECs that were in contact with CMs expressed both BFP and tdT (fig. S19, E and F). These data demonstrate that ECs that are in contact with CMs remain tdT$^+$BFP$^+$, whereas ECs that dissociate with CMs remain tdT$^+$BFP$^-$ when they have undergone EMT or migrate to the liver (fig. S19G). Thus, *tetO-Dre-BFP* enabled us to reveal ongoing cell-cell contacts and their contact history with distinct reporters simultaneously in one mouse (fig. S19H).

## Discussion

We used synNotch modules (*5*, *6*, *10*) to develop an in vivo strategy for monitoring dynamic cell-cell contacts and for tracing cell contact history in mice (table S1 and S2). These two systems can also be applied simultaneously in one mouse if different reporters are selected for separate genetic readouts, enabling both monitoring of ongoing cell-cell contacts and tracing of contact history in diverse biological contexts. One question is whether the affinity of synNotch ligand-receptor binding could influence cell-cell dissociation. Previous studies with the synNotch strategy (*5*, *6*, *10*) may alleviate this concern. We also chose a low-affinity version of the αGFP nanobody LaG17 (*24*) to further mitigate this concern. We studied cardiac tissues because the developing heart offers clear spatial segregation and cell fate transitions to test the performance of our system with a natural readout in a physiological context (Fig. 2B). A second example of endocardial ECs' migration away from the heart to the liver bud and subsequent contribution to the liver vasculature supports the observation of a natural development program (*31*) by our gTCCC system (Fig. 2J). Direct cell-cell contact is needed to activate synNotch, because both the sender lysate and purified mGFP failed to activate the synNotch system in receiver cells (fig. S6), consistent with previous studies showing that the mechanical force exerted by sender cells through contact is required for Notch activation in receiver cells (*5*, *39*). It should also be noted that some cellular contact may not necessarily induce physiological cell-cell communications or regulation of cell fate plasticity. The biological significance of the migration of endocardial cells to the liver and the outgrowth of tumor blood vessels merits further investigation, but these results are a good demonstration of what the technology described here can do.

The dynamic monitoring capacity of our gLCCC system uncovered dynamic interactions of ECs with other cell lineages in development, tissue homeostasis, and pathological conditions. The tracing ability of the gTCCC system detected the contribution of endocardial cells to liver vasculature and tumor vessel outgrowth. The reporter readouts of gLCCC and gTCCC differ in sensitivity, because the reporter in gLCCC reflects the strength of tTA-mediated gene activation, whereas the reporter in gTCCC is a binary readout after permanent recombination and is ubiquitously active due to the Rosa26-CAG promoter (table S1 and S2). In this study, we also generated three special mouse lines for Cre-induced expression of synNotch ligand or receptor. Although the *R26-mGFP* and *H11-αGFP-N-tTA* mouse lines enable synNotch ligand and receptor expression, respectively, in any type of cell with a Cre driver, Tigre-synNotch further made possible ligand and receptor expression in Cre$^+$ cells and all other Cre$^-$ cells in one mouse line, allowing us to explore the cell-cell contact map broadly without predefined cell types in advance (table S1). Contact-dependent labeling could also be useful for studying stem cell–niche cell interactions and their functions in normal and disease contexts. In addition to unraveling cell-cell communication, the contact-dependent cell tracing demonstrated here also offers a potential new method for cell fate mapping in vivo, providing positional information on cells that migrate away from their origins and/or adopt a new fate during development, homeostasis, regeneration, and disease.

## REFERENCES AND NOTES


1. R. Daneman, L. Zhou, A. A. Kebede, B. A. Barres, Pericytes are required for blood-brain barrier integrity during embryogenesis. *Nature* **468**, 562–566 (2010). doi: 10.1038/nature09513; pmid: 20944625
2. D. P. Hoytema van Konijnenburg *et al*., Intestinal epithelial and intraepithelial T cell crosstalk mediates a dynamic response to infection. *Cell* **171**, 783–794.e13 (2017). doi: 10.1016/j.cell.2017.08.046; pmid: 28942917
3. E. C. Butcher, L. J. Picker, Lymphocyte homing and homeostasis. *Science* **272**, 60–66 (1996). doi: 10.1126/science.272.5258.60; pmid: 8600538
4. F. R. Balkwill, M. Capasso, T. Hagemann, The tumor microenvironment at a glance. *J. Cell Sci.* **125**, 5591–5596 (2012). doi: 10.1242/jcs.116392; pmid: 23420197
5. L. Morsut *et al*., Engineering customized cell sensing and response behaviors using synthetic Notch receptors. *Cell* **164**, 780–791 (2016). doi: 10.1016/j.cell.2016.01.012; pmid: 26830878
6. K. T. Roybal *et al*., Engineering T cells with customized therapeutic response programs using synthetic Notch receptors. *Cell* **167**, 419–432.e16 (2016). doi: 10.1016/j.cell.2016.09.011; pmid: 27693353
7. L. He, J. Huang, N. Perrimon, Development of an optimized synthetic Notch receptor as an in vivo cell-cell contact sensor. *Proc. Natl. Acad. Sci. U.S.A.* **114**, 5467–5472 (2017). doi: 10.1073/pnas.1703205114; pmid: 28490499
8. G. Pasqual *et al*., Monitoring T cell-dendritic cell interactions in vivo by intercellular enzymatic labelling. *Nature* **553**, 496–500 (2018). doi: 10.1038/nature25442; pmid: 29342141
9. T. C. Branon *et al*., Efficient proximity labeling in living cells and organisms with TurboID. *Nat. Biotechnol.* **36**, 880–887 (2018). doi: 10.1038/nbt.4201; pmid: 30125270
10. S. Toda, L. R. Blauch, S. K. Y. Tang, L. Morsut, W. A. Lim, Programming self-organizing multicellular structures with synthetic cell-cell signaling. *Science* **361**, 156–162 (2018). doi: 10.1126/science.aat0271; pmid: 29853554
11. Y. Ge *et al*., Enzyme-mediated intercellular proximity labeling for detecting cell–cell interactions. *J. Am. Chem. Soc.* **141**, 1833–1837 (2019). doi: 10.1021/jacs.8b10286; pmid: 30676735
12. J. Wang *et al*., Time-resolved protein activation by proximal decaging in living systems. *Nature* **569**, 509–513 (2019). doi: 10.1038/s41586-019-1188-1; pmid: 31068699
13. L. Ombrato *et al*., Metastatic-niche labelling reveals parenchymal cells with stem features. *Nature* **572**, 603–608 (2019). doi: 10.1038/s41586-019-1487-6; pmid: 31462798
14. R. N. Germain, T-cell development and the CD4-CD8 lineage decision. *Nat. Rev. Immunol.* **2**, 309–322 (2002). doi: 10.1038/nri798; pmid: 12033737
15. C. K. Lee *et al*., Tumor metastasis to lymph nodes requires YAP-dependent metabolic adaptation. *Science* **363**, 644–649 (2019). doi: 10.1126/science.aav0173; pmid: 30733421
16. I. Mellman, G. Coukos, G. Dranoff, Cancer immunotherapy comes of age. *Nature* **480**, 480–489 (2011). doi: 10.1038/nature10673; pmid: 22193102
17. E. Tran *et al*., Cancer immunotherapy based on mutation-specific CD4+ T cells in a patient with epithelial cancer. *Science* **344**, 641–645 (2014). doi: 10.1126/science.1251102; pmid: 24812403
18. A. Pardo-Saganta *et al*., Parent stem cells can serve as niches for their daughter cells. *Nature* **523**, 597–601 (2015). doi: 10.1038/nature14553; pmid: 26147083
19. T. Kadesch, Notch signaling: The demise of elegant simplicity. *Curr. Opin. Genet. Dev.* **14**, 506–512 (2004). doi: 10.1016/j.gde.2004.07.007; pmid: 15380241
20. R. Kopan, M. X. Ilagan, The canonical Notch signaling pathway: Unfolding the activation mechanism. *Cell* **137**, 216–233 (2009). doi: 10.1016/j.cell.2009.03.045; pmid: 19379690
21. D. Sprinzak *et al*., Cis-interactions between Notch and Delta generate mutually exclusive signalling states. *Nature* **465**, 86–90 (2010). doi: 10.1038/nature08959; pmid: 20418862
22. K. T. Roybal *et al*., Precision tumor recognition by T cells with combinatorial antigen-sensing circuits. *Cell* **164**, 770–779 (2016). doi: 10.1016/j.cell.2016.01.011; pmid: 26830879
23. S. Srivastava *et al*., Logic-gated ROR1 chimeric antigen receptor expression rescues T cell-mediated toxicity to normal

tissues and enables selective tumor targeting. *Cancer Cell* **35**, 489–503.e8 (2019). doi: 10.1016/j.ccell.2019.02.003; pmid: 30889382
24. P. C. Fridy *et al*., A robust pipeline for rapid production of versatile nanobody repertoires. *Nat. Methods* **11**, 1253–1260 (2014). doi: 10.1038/nmeth.3170; pmid: 25362362
25. P. A. Furth *et al*., Temporal control of gene expression in transgenic mice by a tetracycline-responsive promoter. *Proc. Natl. Acad. Sci. U.S.A.* **91**, 9302–9306 (1994). doi: 10.1073/pnas.91.20.9302; pmid: 7937760
26. X. Tian *et al*., Subepicardial endothelial cells invade the embryonic ventricle wall to form coronary arteries. *Cell Res.* **23**, 1075–1090 (2013). doi: 10.1038/cr.2013.83; pmid: 23797856
27. M. Vooijs *et al*., Mapping the consequence of Notch1 proteolysis in vivo with NIP-CRE. *Development* **134**, 535–544 (2007). doi: 10.1242/dev.02733; pmid: 17215306
28. Z. Zhu, T. Zheng, C. G. Lee, R. J. Homer, J. A. Elias, Tetracycline-controlled transcriptional regulation systems: Advances and application in transgenic animal modeling. *Semin. Cell Dev. Biol.* **13**, 121–128 (2002). doi: 10.1016/S1084-9521(02)00018-6; pmid: 12127145
29. G. Friedrich, P. Soriano, Promoter traps in embryonic stem cells: A genetic screen to identify and mutate developmental genes in mice. *Genes Dev.* **5**, 1513–1523 (1991). doi: 10.1101/gad.5.9.1513; pmid: 1653172
30. J. L. de la Pompa, J. A. Epstein, Coordinating tissue interactions: Notch signaling in cardiac development and disease. *Dev. Cell* **22**, 244–254 (2012). doi: 10.1016/j.devcel.2012.01.014; pmid: 22340493
31. H. Zhang *et al*., Genetic lineage tracing identifies endocardial origin of liver vasculature. *Nat. Genet.* **48**, 537–543 (2016). doi: 10.1038/ng.3536; pmid: 27019112
32. P. Carmeliet, R. K. Jain, Molecular mechanisms and clinical applications of angiogenesis. *Nature* **473**, 298–307 (2011). doi: 10.1038/nature10144; pmid: 21593862
33. M. Potente, T. Mäkinen, Vascular heterogeneity and specialization in development and disease. *Nat. Rev. Mol. Cell Biol.* **18**, 477–494 (2017). doi: 10.1038/nrm.2017.36; pmid: 28537573
34. M. Potente, H. Gerhardt, P. Carmeliet, Basic and therapeutic aspects of angiogenesis. *Cell* **146**, 873–887 (2011). doi: 10.1016/j.cell.2011.08.039; pmid: 21925313
35. B. Tasic *et al*., Site-specific integrase-mediated transgenesis in mice via pronuclear injection. *Proc. Natl. Acad. Sci. U.S.A.* **108**, 7902–7907 (2011). doi: 10.1073/pnas.1019507108; pmid: 21464299
36. H. Zeng *et al*., An inducible and reversible mouse genetic rescue system. *PLOS Genet.* **4**, e1000069 (2008). doi: 10.1371/journal.pgen.1000069; pmid: 18464897
37. Y. Y. Kisanuki *et al*., Tie2-Cre transgenic mice: A new model for endothelial cell-lineage analysis in vivo. *Dev. Biol.* **230**, 230–242 (2001). doi: 10.1006/dbio.2000.0106; pmid: 11161575
38. B. Sauer, J. McDermott, DNA recombination with a heterospecific Cre homolog identified from comparison of the pac-c1 regions of P1-related phages. *Nucleic Acids Res.* **32**, 6086–6095 (2004). doi: 10.1093/nar/gkh941; pmid: 15550568
39. W. R. Gordon *et al*., Mechanical allostery: Evidence for a force requirement in the proteolytic activation of Notch. *Dev. Cell* **33**, 729–736 (2015). doi: 10.1016/j.devcel.2015.05.004; pmid: 26051539

## ACKNOWLEDGMENTS

We thank Shanghai Biomodel Organism Co., Ltd. for mice generation, our institutional animal facilities for mice husbandry, J. H. Snyder for editing the manuscript, and H. Zeng for providing reporter mice. **Funding:** This work was supported by the Strategic Priority Research Program of the Chinese Academy of Sciences (CAS grant XDA16010507); the CAS Project for Young Scientists in Basic Research (grant YSBR-012); the Shanghai Pilot Program for Basic Research – CAS, Shanghai Branch (grant JCYJ-SHFY-2021-0); the National Science Foundation of China (grants 32050087, 82088101, 91849202, 31730112, 31922032, 81872241, 91639302, and 31701292); the National Key Research & Development Program of China (grants 2019YFA0110403, 2019YFA0802000, 2018YFA0107900, 2018YFA0108100, 2019YFA0802803,and 2020YFA0803202); the Shanghai Science and Technology Commission (grants 19JC1415700, 19ZR1479800, 20QC1401000, and 20200CXJQ01); funds from the Mildred V. Strouss Trust and the Tobacco-Related Disease Research Program (28IR-0067) to R.A.W.; and an XPLORER PRIZE from the Tencent Foundation. **Author contributions:** S.Z. designed the study, performed the experiments, and analyzed the data. H.Zha., Z.L., K.L., H.Zhu, W.P., and L.H. bred the mice, performed the experiments, and discussed the work. R.A.W. provided intellectual input and revised and edited the manuscript. B.Z. conceived and supervised the study and wrote the manuscript. **Competing interests:** The authors declare no competing interests. **Data and materials availability:** The RNA-sequencing data generated in his study have been deposited in the NCBI Sequence Read Archive under BioProject ID PRJNA866292. Transgenic mice generated in this study are available from B.Z. under a material transfer agreement with the CAS Center for Excellence in Molecular Cell Science. 

## SUPPLEMENTARY MATERIALS

science.org/doi/10.1126/science.abo5503
Materials and Methods
Figs. S1 to S19
Tables S1 and S2
References (*40*–*53*)
MDAR Reproducibility Checklist

View/request a protocol for this paper from *Bio-protocol*.

Submitted 12 February 2022; accepted 26 October 2022
10.1126/science.abo5503

Science

# Monitoring of cell-cell communication and contact history in mammals

Shaohua ZhangHuan ZhaoZixin LiuKuo LiuHuan ZhuWenjuan PuLingjuan HeRong A. WangBin Zhou

*Science*, 378 (6623), eabo5503. • DOI: 10.1126/science.abo5503

**Tracing a history of cell-cell contact**

The ability to monitor the history of cell-cell contact could benefit our understanding of cellular interactions in many biological contexts, from development to various disease states. Zhang *et al*. modified synthetic receptor systems that could be targeted to cells of interest in mice. Binding of the designed ligand on a sender cell to a compatible receptor on a receiver cell permanently marked the receiver cell through a change in expression of a fluorescent reporter. For example, they could detect endothelial cells that moved during development from the heart to the liver. —LBR







*Science* (ISSN ) is published by the American Association for the Advancement of Science. 1200 New York Avenue NW, Washington, DC 20005. The title *Science* is a registered trademark of AAAS.